

Capacitor-Voltage Regulation and Linear-Range Extension of a Hybrid Cascaded Modular Multilevel Converter

Xianghua Shi¹, Steven Howell^{1,2}, Curtis Shumski¹, Shaahin Filizadeh^{1*}, David Jacobson²

¹ Department of Electrical and Computer Engineering, University of Manitoba, 75A Chancellor's Circle, Winnipeg, MB, Canada

² System Planning Department, Manitoba Hydro, 820 Taylor Ave, Winnipeg, MB, Canada

* shaahin.filizadeh@umanitoba.ca

Abstract: This paper presents a study of the hybrid cascaded modular multilevel converter (HC-MMC). It shows that voltage regulation of the full-bridge submodules requires special provisions for energy-flow control between the converter's main power stage and the external ac network. Novel control and hardware methods for regulating the converter's submodule voltage and extending its linear operating range are presented. The mathematical foundations of these methods are developed using simplified converter models. Experimental results using a laboratory prototype are presented to verify the efficacy of these methods. Extensive electromagnetic transient simulation studies are also conducted to verify the proposed solutions' effectiveness in normal operating conditions as well as under dc faults.

1. Introduction

Modular multilevel converters (MMCs) have become prevalent in areas where conventional two- and multilevel voltage-source converters (VSCs) were traditionally used. MMCs provide a high level of controllability, improved harmonic performance, and low losses in scalable topologies that can be adapted to the ratings of each application [1]-[8]. In the context of high-voltage dc (HVDC) systems, MMCs offer reduced filtering requirements, immunity to commutation failure, and wider operating ranges compared with line-commutated converters (LCCs) [9].

The original MMC topology is based upon half-bridge (HB) submodules and has been extensively studied for high-power applications including HVDC transmission, integration of renewable energy sources, and motor drives [10]-[12]. Despite its benefits, the HB-MMC topology is unable to block dc faults, which is a severe drawback. In the event of a dc fault, the HB submodules are blocked; however, the ac system continues to feed the faulted dc side through the reverse-conducting submodule diodes. To prevent this, ac circuit breakers must operate and isolate the ac system from the faulted dc system.

A new class of MMC topologies have been proposed with the ability to block dc faults [13]-[21]. These converters deploy full-bridge (FB) submodules in their topologies, either as the only building block or in combination with HB submodules [14], [15] or other controlled switching configurations [14], [20], [21]. The advantage of using FB submodules is that upon blocking in the event of a fault, the FB submodule capacitors will remain in the circuit's conduction path. The stack of FB-submodule capacitors will continue to charge, thus opposing the ac system's voltage and countering its contribution to a dc fault, thereby providing dc-fault blocking.

This article has been accepted for publication in a future issue of this journal, but has not been fully edited.

Content may change prior to final publication in an issue of the journal. To cite the paper please use the doi provided on the Digital Library page.

This paper considers one such hybrid MMC in which a stack of FB submodules is placed in series with each phase [15] as shown in Fig. 1(a). The paper firstly examines the converter's operation from the standpoints of average power and submodule capacitor voltage balancing/regulation. This analysis demonstrates that special provisions are required to ensure that the FB submodule capacitors retain their desired average voltage throughout the converter's entire operating range. The paper then presents methodologies for achieving FB-submodule capacitor voltage regulation. The proposed methods are based upon control system modifications to regulate the FB submodule capacitor voltages and to extend the converter's linear operating range. A novel topological solution is also proposed that further extends the converter's linear operating range. The proposed solutions are established analytically using simplified converter models. Experimental results obtained on a laboratory prototype are then presented to validate the proposed voltage regulation methods. Extensive electromagnetic transient (EMT) simulations are also conducted to fully assess their functionality during normal operation and dc-fault conditions for a mixed-technology (LCC-MMC) dc transmission system.

2. Operating Principles of the HC-MMC

A single-phase schematic diagram of the HC-MMC is shown in Fig. 1(a). The converter consists of two building blocks: the main power stage, which is similar to a conventional HB-MMC, and the active-filter stage comprised of FB submodules. The main power stage is primarily responsible for generating a controlled voltage at its terminals (denoted with subscript 'm' in Fig. 1(a)) and for transmitting power between the dc and ac sides. The stack of FB submodules is utilized as an active filter to reduce harmonics and block dc faults. The HB submodules in the main power stage have a nominal voltage of $V_{c-hb} = V_{dc}/N_h$, where V_{dc} is the dc-link voltage and N_h is the number of arm submodules (excluding redundancy). To prevent the ac system's contribution to a dc fault, FB-submodule capacitors must maintain a (minimum) nominal voltage of $V_{c-fb} = (V_{dc}/2)/N_f$ where N_f is the number of FB submodules (excluding redundancy) per phase when the peak ac voltage is assumed to be $V_{dc}/2$.

In this paper, phase-disposition PWM (PD-PWM) [1], [2] is used for both the main power stage and the active filter stage. Since the stack of FB submodules provides filtering for the main power stage voltage, they must use high-frequency PD-PWM, whereas a low-frequency PD-PWM is sufficient for the main power stage. The HB submodules can produce two voltage levels: 0 and V_{c-hb} . The FB submodules can produce three voltage levels: 0 and $\pm V_{c-fb}$ [15]. Without considering voltage-regulation control for the stacked FB submodules, the basic operating waveforms for the HC-MMC with $N_h = 6$ and $N_f = 3$ using PD-PWM are shown in Fig. 1(b), where v_{ref-ph} , $v_{ref-main}$, and v_{ref-fb} are the references for the output phase voltage, the main power stage voltage, and the FB stack voltage respectively. The frequency of the carriers

This article has been accepted for publication in a future issue of this journal, but has not been fully edited.

Content may change prior to final publication in an issue of the journal. To cite the paper please use the doi provided on the Digital Library page.

for the main power stage and the stacked FB submodules are $9f_o$ (low-frequency) and $27f_o$ (high-frequency), respectively, where f_o denotes the fundamental frequency. It is observed that the actual voltage waveform of v_{am} is unable to track its reference ($v_{ref-main}$) when the instantaneous value of $v_{ref-main}$ becomes larger than 1.0. However, the terminal output phase voltage (v_a) can be made sinusoidal by the FB submodules to compensate for the lack of tracking by the main power stage with $v_{ref-fb} = v_{ref-ph} - v_{am}$. Without voltage-regulation control for the stacked FB submodules, the same reference waveform must be used for both the output phase voltage and the main power stage voltage to achieve the least filtering burden for the stacked FB submodules. However, this will cause energy deficiency for the main power stage when the modulation index is larger than 1.0 and leads to a voltage drop in the FB-submodule capacitor voltages (which will be analyzed in detail in Section 3).

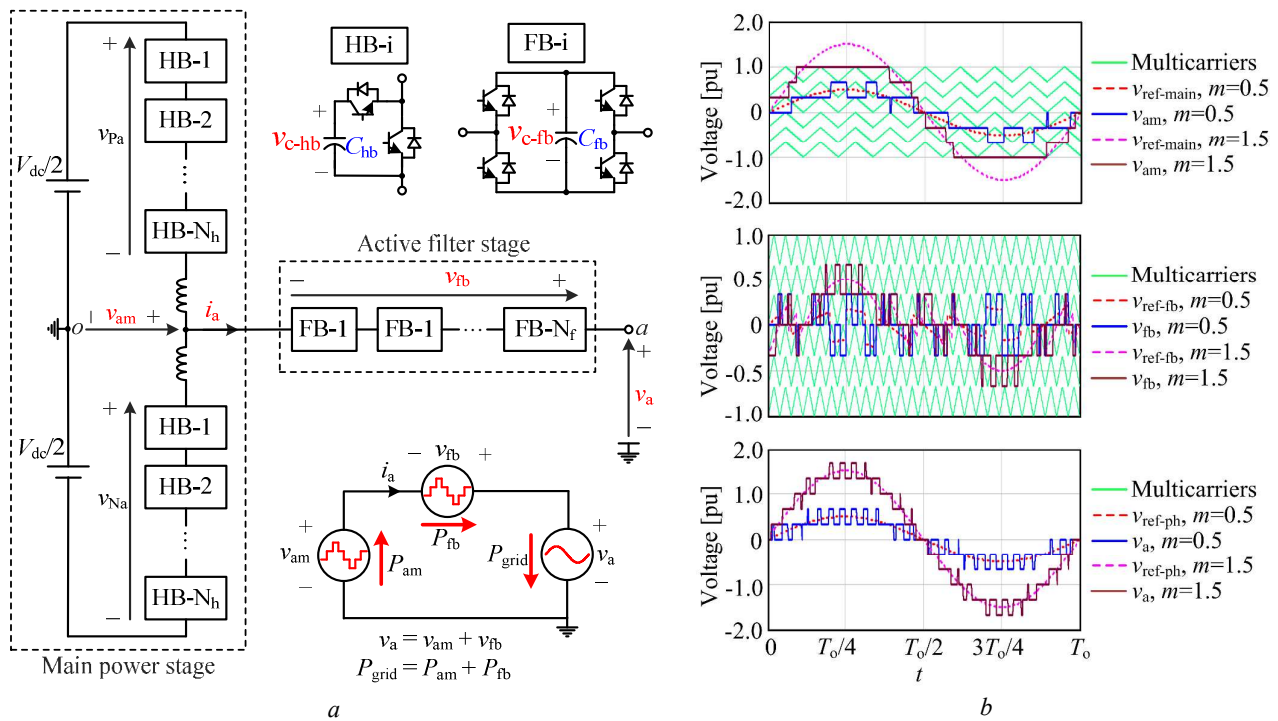


Fig. 1. HC-MMC topology and ideal basic waveforms

a. Schematic diagram of the single-phase HC-MMC circuit

b. Basic waveforms operating with PD-PWM without considering voltage-regulation control

The HC-MMC provides several degrees of freedom for crafting output voltages that meet harmonic requirements. The THD of the output voltage depends upon the numbers of both HB and FB submodules, among other factors. It is shown that with 3-level PD-PWM switching for the FB submodules, the output voltage THD will be lower than that of the main power stage voltage if $N_f > N_h/2$. In other words, the number of FB submodules must be at least half of the number of HB submodules in the main power stage

This article has been accepted for publication in a future issue of this journal, but has not been fully edited.

Content may change prior to final publication in an issue of the journal. To cite the paper please use the doi provided on the Digital Library page.

[23]. In the experiments presented in this paper, the quantities of submodules are selected to satisfy this condition.

3. Capacitor-Voltage Regulation and Linear-Range Extension Methods

During normal operation, the HB- and FB-submodule capacitor voltages must be well balanced and maintained tightly around their nominal values. In order to balance the submodule-capacitor voltages, the conventional sorting and rotating method was implemented [22]. To balance the capacitor voltages within each stage, the sort and rotate method is implemented separately for both the main power stage and the active filter stage. For the HB submodules within the main power stage, this method of operation, which guarantees N_h submodules are inserted at every instant of time, helps ensure that the HB submodule-capacitor voltages remain balanced and regulated at their nominal value (V_{dc}/N_h) based upon Kirchhoff's voltage law ($V_{dc} = V_{Pa} + V_{Na} = N_h \cdot V_{c-hb}$). There is, however, no such inherent regulating mechanism to ensure that the average FB submodule capacitor voltages remain at their desired nominal value of $V_{dc}/(2N_f)$, which is the minimum requirement for dc-fault blocking. Therefore, a control system is required to regulate the average FB-submodule capacitor voltages.

The following subsection provides an analysis of the average power delivered by the FB submodules under idealized conditions. This analysis reveals the underlying conditions for power balance and hence voltage regulation for FB submodule capacitors. Voltage regulation methods will then be developed based upon the conclusions of power balance analysis.

3.1. Average Power Analysis

Assume that the number of submodules in each stage is sufficiently large and that all submodules are balanced so that the converter output voltage is essentially sinusoidal. Therefore, the output phase voltage, v_a , and phase current, i_a , are expressed as follows.

$$\begin{aligned} v_a(t) &= m \frac{V_{dc}}{2} \sin(\omega_0 t) \\ i_a(t) &= I_m \sin(\omega_0 t - \varphi) \quad \varphi \in [-\pi/2, \pi/2] \end{aligned} \quad (1)$$

where m is the converter's modulation index, I_m is the peak of phase current, φ is the phase difference between voltage and current ($\cos(\varphi) \geq 0$ for inverter mode of operation), and ω_0 is the fundamental angular frequency. The average power absorbed by the ac grid is as follows.

$$\begin{aligned} P_{\text{grid}}(m) &= \frac{1}{T_0} \int_0^{T_0} v_a(t) \cdot i_a(t) dt = \frac{1}{T_0} \int_0^{T_0} m \frac{V_{dc}}{2} \sin(\omega_0 t) \cdot I_m \sin(\omega_0 t - \varphi) dt \\ &= \frac{m V_{dc} I_m \cos(\varphi)}{4} \end{aligned} \quad (2)$$

This article has been accepted for publication in a future issue of this journal, but has not been fully edited.

Content may change prior to final publication in an issue of the journal. To cite the paper please use the doi provided on the Digital Library page.

The average power delivered by the main power stage depends on the voltage, v_{am} , and the phase current, i_a , at its terminals. Since the largest voltage crafted by the main power stage is $V_{dc}/2$, the voltage v_{am} is purely sinusoidal only when $m \leq 1.0$ and will be clipped at $V_{dc}/2$ when $m > 1.0$. Therefore, two distinct cases are identified to calculate the average power delivered by the main power stage.

Case 1: $m \leq 1.0$

For this case $v_{am}(t) = v_a(t)$ and as such $v_{fb}(t) = v_{ref}(t) - v_{am}(t) = 0$; therefore, the average power delivered by the main power stage is equal to the power absorbed by the ac grid:

$$P_{am}(m) = P_{grid}(m) = \frac{mV_{dc}I_m \cos(\varphi)}{4} \quad (3)$$

Thus, the average power delivered by the FB submodules is $P_{fb}(m) = P_{grid}(m) - P_{am}(m) = 0$, which means for $m \leq 1.0$ the stack of FB submodules will not exchange any net real power with the ac grid and hence will not experience any voltage deviations from their nominal value.

Case 2: $m > 1.0$

For this case, the voltage crafted by the main power stage will be clipped as shown in Fig. 2(a) (shown for $m = 1.2$). Therefore,

$$v_{am}(t) = \frac{V_{dc}}{2} \begin{cases} +1 & \text{if } \omega_0 t \in [\alpha, \pi - \alpha] \\ -1 & \text{if } \omega_0 t \in [\pi + \alpha, 2\pi - \alpha] \\ m \sin(\omega_0 t) & \text{otherwise} \end{cases} \quad (4)$$

where $\alpha = \sin^{-1}(1/m)$. The resulting voltage across the stack of FB submodules is shown below.

$$v_{fb}(t) = v_a(t) - v_{am}(t) = \frac{V_{dc}}{2} \begin{cases} m \sin(\omega_0 t) - 1 & \text{if } \omega_0 t \in [\alpha, \pi - \alpha] \\ m \sin(\omega_0 t) + 1 & \text{if } \omega_0 t \in [\pi + \alpha, 2\pi - \alpha] \\ 0 & \text{otherwise} \end{cases} \quad (5)$$

In this case, the average power delivered by the main power stage and the stack of FB submodules are respectively expressed as follows.

$$\begin{aligned} P_{am}(m) &= \frac{1}{T_o} \int_0^{T_o} v_{am}(t) \cdot i_a(t) dt \\ &= \frac{1}{2\pi} \left[\int_0^{\alpha} m \frac{V_{dc}}{2} \sin(\theta) \cdot I_m \sin(\theta - \varphi) d\theta + \int_{\alpha}^{\pi - \alpha} \frac{V_{dc}}{2} \cdot I_m \sin(\theta - \varphi) d\theta + \int_{\pi - \alpha}^{\pi + \alpha} m \frac{V_{dc}}{2} \sin(\theta) \cdot I_m \sin(\theta - \varphi) d\theta \right. \\ &\quad \left. + \int_{\pi + \alpha}^{2\pi - \alpha} -\frac{V_{dc}}{2} \cdot I_m \sin(\theta - \varphi) d\theta + \int_{2\pi - \alpha}^{2\pi} m \frac{V_{dc}}{2} \sin(\theta) \cdot I_m \sin(\theta - \varphi) d\theta \right] \\ &= \frac{V_{dc} I_m \cos(\varphi)}{2\pi} \left(\frac{\sqrt{m^2 - 1}}{m} + m \sin^{-1} \left(\frac{1}{m} \right) \right) \end{aligned} \quad (6)$$

This article has been accepted for publication in a future issue of this journal, but has not been fully edited.

Content may change prior to final publication in an issue of the journal. To cite the paper please use the doi provided on the Digital Library page.

$$P_{fb}(m) = P_{grid}(m) - P_{am}(m) = \frac{V_{dc} I_m \cos(\varphi)}{2\pi} \left(\frac{\pi m}{2} - \frac{\sqrt{m^2 - 1}}{m} - m \sin^{-1}\left(\frac{1}{m}\right) \right) \quad (7)$$

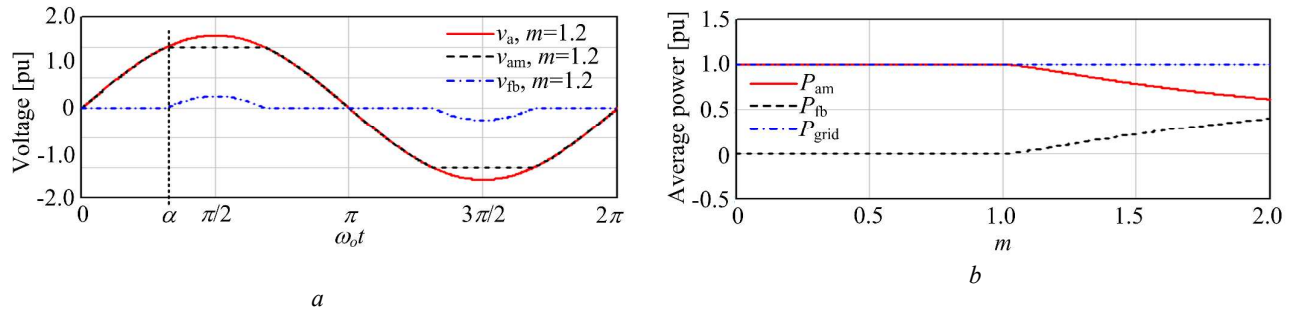


Fig. 2. HC-MMC operation under ideal conditions

a. Voltage waveforms (v_{am} , v_{fb} and v_a) with $m = 1.2$ under ideal conditions

b. Average power (P_{am} , P_{fb} and P_{grid}) as a function of m

According to the above analysis, Fig. 2(b) shows the variations of real power for the main power stage and the stack of FB submodules (both normalized by the power absorbed by the ac grid, $P_{grid}(m)$) as a function of modulation index. For $m > 1.0$ the stack of FB submodules delivers real power to the ac grid, thereby experiencing a net energy deficiency that will manifest as a FB submodule capacitor voltage depression.

3.2. Capacitor Voltage Regulation Schemes for FB Submodules

The main reason for the FB-submodule capacitor voltage depression is that the main power stage does not deliver enough average power to the ac network when the main power stage uses the same voltage reference as the phase v_a and operates with $m > 1.0$. A method for FB submodule capacitor voltage regulation using a trapezoidal PWM method is given in [24], and is briefly described in Section 3.2.1. However, this method suffers from the low-frequency harmonics embedded in its trapezoidal reference, which yield a large THD (see Section 3.3). In view of this shortcoming, two new voltage-regulation methods are proposed in Sections 3.2.2 and 3.2.3. The two proposed methods not only improve the THD of v_{am} but also extend the linear operating range of the converter.

3.2.1 Trapezoidal PWM with variable slope: One method to compensate the energy deficiency in the FB submodules is to use a slope-adjustable trapezoidal PWM for the main power stage [24], as shown in Figs. 3(a) and (b), where $v_{cref-fb}$ and $v_{cavg-fb}$ are the reference and average capacitor voltages of the FB submodules in the active-filter stage. The detailed derivations based on the zero-net energy absorbed by the stacked FB submodules are shown in [24]. However, [24] only analyzes the relationship between the slope of the trapezoidal reference, k_{trap} , and its equivalent fundamental component when $k_{trap} > 2\omega_o/\pi$ (i.e.,

This article has been accepted for publication in a future issue of this journal, but has not been fully edited.

Content may change prior to final publication in an issue of the journal. To cite the paper please use the doi provided on the Digital Library page.

$m > 8/\pi^2$), for which the reference is trapezoidal. Note that for $k_{\text{trap}} < 2\omega_o/\pi$ (or $m < 8/\pi^2$), the reference becomes a triangular waveform with a peak below unity (see waveforms for $m = 0.7$ in Fig. 3(a)). The expressions for the trapezoidal reference for these two cases are as follows.

$$v_{\text{am}}(t) = \frac{V_{\text{dc}}}{2} \begin{cases} k_{\text{trap}} t, & t \in [0, T_o/4] \cup [3T_o/4, T_o] \\ -k_{\text{trap}}(t - T_o/4), & t \in [T_o/4, 3T_o/4] \end{cases} \quad \text{if } k_{\text{trap}} \leq \frac{2\omega_o}{\pi};$$

$$v_{\text{am}}(t) = \frac{V_{\text{dc}}}{2} \begin{cases} k_{\text{trap}} t, & t \in [0, 1/k_{\text{trap}}] \cup [T_o - 1/k_{\text{trap}}, T_o] \\ -k_{\text{trap}}(t - T_o/2 + 1/k_{\text{trap}}), & t \in [T_o/2 - 1/k_{\text{trap}}, T_o/2 + 1/k_{\text{trap}}] \\ 1, & t \in [1/k_{\text{trap}}, T_o/2 - 1/k_{\text{trap}}] \\ -1, & t \in [T_o/2 + 1/k_{\text{trap}}, T_o - 1/k_{\text{trap}}] \end{cases} \quad \text{if } k_{\text{trap}} > \frac{2\omega_o}{\pi} \quad (8)$$

According to the detailed analysis of the trapezoidal PWM method in [24], the relationship between the converter modulation index, m , and the slope of the trapezoidal waveform, k_{trap} , is expressed as

$$m = \begin{cases} \frac{8k_t}{\pi^2} & \text{if } 0 < k_t \leq 1 \\ \frac{8k_t}{\pi^2} \sin\left(\frac{\pi}{2k_t}\right) & \text{if } k_t > 1 \end{cases} \quad (9)$$

where $k_t = k_{\text{trap}}/(2\omega_o/\pi)$. The relationship between k_t and m is plotted in Fig. 4(a) based upon the expression in (9). It is observed that the relationship between the control variable (k_t) and the modulation index is nonlinear for $m > 8/\pi^2$ with a maximum modulation index of $4/\pi$.

3.2.2 Modified sinusoidal PWM with range extension: As seen from Fig. 2(b), for $m > 1.0$ the main power stage does not deliver all of the average power required by the ac grid. To resolve this issue, the modulation index of the main power stage is separated from the converter's output-voltage modulation index (m) and is denoted as $m_{\text{new}} = m + \Delta m$ as shown in Fig. 3(c) with $m_{\text{mpk}} = 1$, where m_{mpk} corresponds to the peak value of the voltage crafted by the main power stage normalized by $V_{\text{dc}}/2$. For $m > 1.0$, a control system judiciously adjusts Δm to ensure that the required real power is provided to the ac grid entirely by the main power stage and not in conjunction with the FB stack.

The average power delivered by the main power stage (in (6)) must be recalculated using m_{new} to replace m . Then the power delivered by the FB submodules, which must be equal to zero for FB submodule capacitor-voltage regulation, is as follows.

This article has been accepted for publication in a future issue of this journal, but has not been fully edited.

Content may change prior to final publication in an issue of the journal. To cite the paper please use the doi provided on the Digital Library page.

$$\begin{aligned}
 P_{fb} &= P_{grid}(m) - P_{am}(m_{new}) = 0 \\
 \Rightarrow \frac{mV_{dc}I_m \cos(\varphi)}{4} - \frac{V_{dc}I_m \cos(\varphi)}{2\pi} \left(\frac{\sqrt{m_{new}^2 - 1}}{m_{new}} + m_{new} \sin^{-1}\left(\frac{1}{m_{new}}\right) \right) &= 0 \\
 \Rightarrow m &= \frac{2}{\pi} \left[\frac{\sqrt{m_{new}^2 - 1}}{m_{new}} + m_{new} \sin^{-1}\left(\frac{1}{m_{new}}\right) \right]
 \end{aligned} \tag{10}$$

The above expression obtained from the average power analysis readily demonstrates how to adjust the modulation index for the main power stage, m_{new} , such that the power exchange with FB submodules is zero, and thus their voltage remains regulated at the desired value.

Based on (10), Fig. 4(b) shows the relationship between m and both m_{new} and Δm . A maximum modulation index of $4/\pi$ is achieved and the linear range is extended to 1.0 (as opposed to the trapezoidal method's linear range of up to $8/\pi^2$). A closed-loop control system for FB submodule capacitor-voltage regulation based upon this concept is shown in Fig. 3(d) with $m_{mpk} = 1$, wherein Δm augments m to form m_{new} . In general, 3rd harmonic injection can be used for the sinusoidal PWM method to further extend the linear modulation index range. Figure 3(d) shows the proposed control system including 3rd harmonic injection, where k_{3rd} denotes the proportion of the 3rd harmonic added to the fundamental component. The value of k_{3rd} is typically set to 1/6 in order to extend the linear range up to 1.15. Compared with the trapezoidal PWM method, the proposed modified sinusoidal PWM method is capable of injecting 3rd harmonic into the reference voltages. In order to obtain balanced 3rd harmonic in the converter's output 3-phase voltages to eliminate the 3rd harmonic in the line voltages, the amount of 3rd harmonic injected is calculated according to the converter's modulation index (m) instead of m_{new} since m_{new} can be different between phases due to the necessity of independent control of FB-submodule capacitor voltages for each phase.

This article has been accepted for publication in a future issue of this journal, but has not been fully edited.

Content may change prior to final publication in an issue of the journal. To cite the paper please use the doi provided on the Digital Library page.

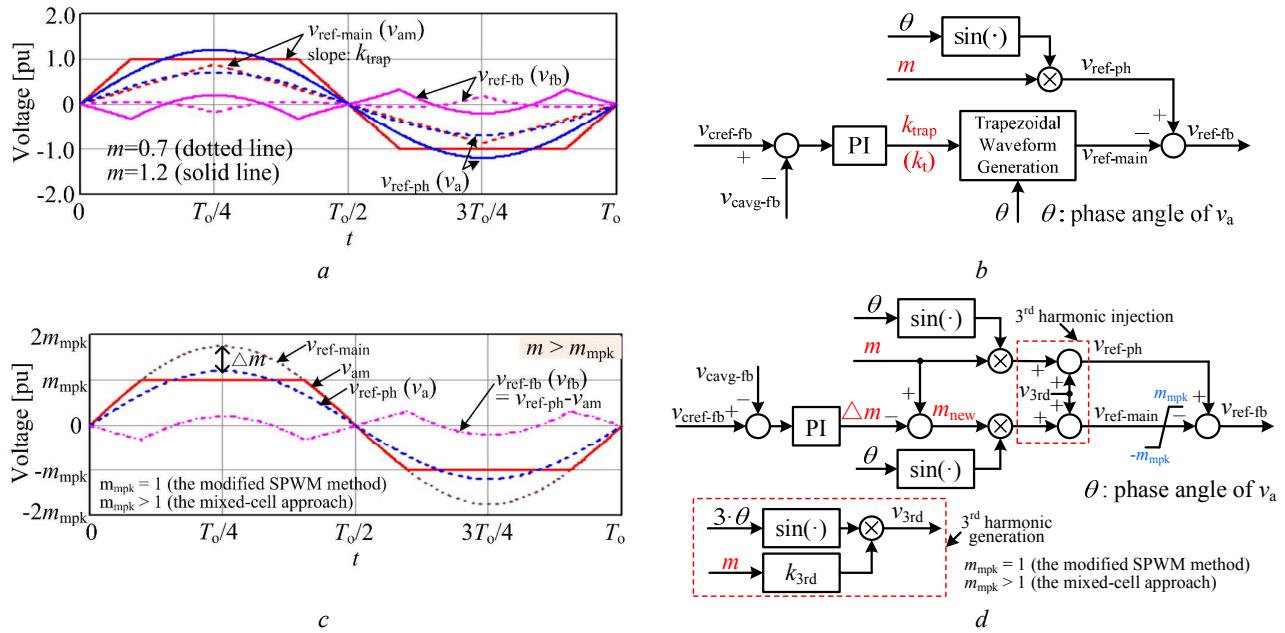


Fig. 3. Trapezoidal and modified sinusoidal PWM methods

a. Reference waveforms under trapezoidal PWM

b. Voltage regulator with the trapezoidal PWM

c. Reference waveforms under the modified sinusoidal PWM ($m_{mpk} = 1$) and the mixed-submodule approach ($m_{mpk} > 1$)

d. Voltage regulator with the modified sinusoidal PWM ($m_{mpk} = 1$) and the mixed-submodule approach ($m_{mpk} > 1$)

3.2.3 Mixed-submodule converter topology: To further extend the linear operating range of the HC-MMC beyond the modulation index of 1.0, additional FB submodules are used in the main power stage in series with each arm's HB submodules. The linear range is extended because FB submodules can insert negative capacitor voltages whereas HB submodules cannot. The capacitance (denoted as C_{fm}) and capacitor voltage (denoted as V_{c-fm}) of these main power stage FB submodules are the same as those for the HB submodules, i.e., $C_{fm} = C_{hb}$ (shown in Fig. 1(a)) and $V_{c-fm} = V_{c-hb} = V_{dc}/N_h$. Assuming that the number of FB submodules added to the main power stage per arm is N_{fm} , the minimum voltage crafted by the upper arm in the main power stage will be $V_{Pa} = -N_{fm} \cdot V_{c-fm} = -N_{fm} \cdot V_{dc}/N_h$ if all FB submodules in the upper arm are inserted with negative capacitor voltages and all HB submodules are bypassed. Thus, the peak voltage of the main power stage voltage is $V_{dc}/2 - V_{Pa} = (1+2N_{fm}/N_h) \cdot V_{dc}/2$, resulting in an improved main power stage clipping level of $m_{mpk} (= 1+2N_{fm}/N_h)$ as shown in Fig. 3(c) instead of unity as shown in Fig. 2(a).

Table 1 shows the voltage levels of the mixed-submodule converter with $N_h = 6$ and $N_{fm} = 1$, where each level is equal to the nominal submodule-capacitor voltage ($V_{dc}/6$). In Table 1, the voltage levels for v_{Pa} and v_{Na} reflect the number of inserted submodules from the upper and lower arms, respectively, and the negative number indicates the required number of FB submodules inserted with negative capacitor

This article has been accepted for publication in a future issue of this journal, but has not been fully edited.

Content may change prior to final publication in an issue of the journal. To cite the paper please use the doi provided on the Digital Library page.

voltages. From Table 1, it is observed that the peak value of v_{am} is at $4V_{dc}/6$, which is consistent with $(1+2N_{fm}/N_h) \cdot V_{dc}/2$. Furthermore, the equivalent inserted number of submodules with positive capacitor voltage is always N_h for all possible voltage levels of v_{am} . This indicates that the operating mechanism that ensures N_h submodules are inserted for each pair of upper and lower arms is still maintained for the mixed-submodule converter. Therefore, the sorting and rotating method can be used to ensure that the HB and FB submodules in the main power stage of the mixed-submodule converter can be balanced and regulated at their nominal value (V_{dc}/N_h).

Table 1 The voltage levels for the mixed-submodule approach with $N_h = 6$ and $N_{fm} = 1$

Voltage level of v_{pa}	-1	0	1	2	3	4	5	6	7
Voltage level of v_{am} ($=V_{dc}/2-V_{pa}$)	4	3	2	1	0	-1	-2	-3	-4
Voltage level of v_{Na} ($=V_{dc}/2+v_{am}$)	7	6	5	4	3	2	1	0	-1
Equivalent inserted # of submodules	6	6	6	6	6	6	6	6	6

Note: Each voltage level is equal to the nominal submodule-capacitor voltage ($V_{dc}/6$).

Based upon the above analysis for the mixed-submodule approach, the voltage v_{am} is purely sinusoidal when $m \leq m_{mpk}$ and clipped to m_{mpk} when $m > m_{mpk}$. Similar to the analysis in Section 3.1, v_{am} and v_{fb} are as follows:

$$v_{am}(t) = \frac{V_{dc}}{2} \cdot \begin{cases} +m_{mpk} & \text{if } \omega_0 t \in [\alpha, \pi - \alpha] \\ -m_{mpk} & \text{if } \omega_0 t \in [\pi + \alpha, 2\pi - \alpha] \\ m \sin(\omega_0 t) & \text{otherwise} \end{cases} \quad (11)$$

$$v_{fb}(t) = v_a(t) - v_{am}(t) = \frac{V_{dc}}{2} \cdot \begin{cases} m \sin(\omega_0 t) - m_{mpk} & \text{if } \omega_0 t \in [\alpha, \pi - \alpha] \\ m \sin(\omega_0 t) + m_{mpk} & \text{if } \omega_0 t \in [\pi + \alpha, 2\pi - \alpha] \\ 0 & \text{otherwise} \end{cases} \quad (12)$$

where $\alpha = \sin^{-1}(m_{mpk}/m)$ and $m > m_{mpk}$. The average power delivered by the main stage is:

$$\begin{aligned} P_{am}(m) &= \frac{1}{T_o} \int_0^{T_o} v_{am}(t) \cdot i_a(t) dt \\ &= \frac{1}{2\pi} \left[\int_0^\alpha m \frac{V_{dc}}{2} \sin(\theta) \cdot I_m \sin(\theta - \varphi) d\theta + \int_\alpha^{\pi - \alpha} m_{mpk} \cdot \frac{V_{dc}}{2} \cdot I_m \sin(\theta - \varphi) d\theta + \int_{\pi - \alpha}^{\pi + \alpha} m \frac{V_{dc}}{2} \sin(\theta) \cdot I_m \sin(\theta - \varphi) d\theta \right. \\ &\quad \left. + \int_{\pi + \alpha}^{2\pi - \alpha} -m_{mpk} \cdot \frac{V_{dc}}{2} \cdot I_m \sin(\theta - \varphi) d\theta + \int_{2\pi - \alpha}^{2\pi} m \frac{V_{dc}}{2} \sin(\theta) \cdot I_m \sin(\theta - \varphi) d\theta \right] \quad (13) \\ &= \frac{V_{dc} I_m \cos(\varphi) m_{mpk}}{2\pi} \left(\frac{\sqrt{m^2 - m_{mpk}^2}}{m} + \frac{m}{m_{mpk}} \sin^{-1} \left(\frac{m_{mpk}}{m} \right) \right) \end{aligned}$$

Similar to (7), the average power delivered by the stack of FB submodules is desired to be controlled to be zero by the modified sinusoidal PWM method when $m > m_{mpk}$, then:

This article has been accepted for publication in a future issue of this journal, but has not been fully edited. Content may change prior to final publication in an issue of the journal. To cite the paper please use the doi provided on the Digital Library page.

$$\begin{aligned}
 P_{fb} &= P_{grid}(m) - P_{am}(m_{new}) = 0 \\
 \Rightarrow & \frac{mV_{dc}I_m \cos(\varphi)}{4} - \frac{V_{dc}I_m \cos(\varphi)m_{mpk}}{2\pi} \left(\frac{\sqrt{m_{new}^2 - m_{mpk}^2}}{m_{new}} + \frac{m_{new}}{m_{mpk}} \sin^{-1}\left(\frac{m_{mpk}}{m_{new}}\right) \right) = 0 \\
 \Rightarrow & m = \frac{2m_{mpk}}{\pi} \left[\frac{\sqrt{m_{new}^2 - m_{mpk}^2}}{m_{new}} + \frac{m_{new}}{m_{mpk}} \sin^{-1}\left(\frac{m_{mpk}}{m_{new}}\right) \right]
 \end{aligned} \tag{14}$$

Fig. 4(c) illustrates the relationship between m and $\Delta m (= m_{new} - m)$ with different m_{mpk} , and shows that the maximum modulation index is equal to $(4m_{mpk}/\pi)$ and the linear range is extended to m_{mpk} . The ratio of the HB and FB submodules in the main power stage of the mixed-submodule converter is chosen according to the expected linear operating range of the system, i.e., the value of m_{mpk} . For example, if 5% additional FB submodules are added to the main power stage, i.e., $N_{fm}/N_h = 0.05$, the linear range of the converter will be extended by 10%. In general, addition of any submodule must be done according to cost-performance tradeoffs.

Similar to the modified sinusoidal PWM method, the closed-loop control system for the FB-submodule capacitor-voltage regulation is shown in Fig. 3(d) with $m_{mpk} = (1+2N_{fm}/N_h)$. If 3rd harmonic injection is used, the linear modulation index can be extended to $1.15m_{mpk}$. In summary, as seen from Fig. 4, both the trapezoidal and modified sinusoidal PWM methods have a maximum modulation index of $4/\pi$, whereas the mixed-submodule approach has a higher range up to $4m_{mpk}/\pi$. The linear modulation range becomes progressively larger from $8/\pi^2$ (trapezoidal) to 1.0 (modified sinusoidal) and to m_{mpk} (mixed-submodule). If 3rd harmonic injection is used the linear ranges of the modified sinusoidal PWM and the mixed-cell approaches may be increased by an additional 15%.

3.3. THD Analysis of the Main Power Stage Voltage (v_{am})

As described in Section 3.2, the discussed voltage-regulation methods adjust the voltage reference for the main power stage ($v_{ref-main}$), which directly influences the filtering burden of the active-filter stage. In order to evaluate the filtering burden of the FB submodules, the THD of the voltage crafted by the main power stage (v_{am}) is analyzed for the different presented voltage-regulation methods. In general, the THD of a periodic waveform is defined as follows.

$$\text{THD} = \frac{\sqrt{\sum_{h=2}^{\infty} V_{hrms}^2}}{V_{1rms}} = \frac{\sqrt{V_{rms}^2 - V_{1rms}^2}}{V_{1rms}} = \sqrt{\left(\frac{V_{rms}}{V_{1rms}}\right)^2 - 1} \tag{15}$$

This article has been accepted for publication in a future issue of this journal, but has not been fully edited.

Content may change prior to final publication in an issue of the journal. To cite the paper please use the doi provided on the Digital Library page.

where V_{rms} and $V_{h\text{rms}}$ are the root mean square (RMS) of the waveform and the h -th harmonic component, respectively.

For the trapezoidal PWM method, the RMS values of the trapezoidal waveform (expressed in (8)) and its fundamental component are as follows.

$$V_{\text{trap_rms}}^2 = \frac{2}{T_o} \int_0^{T_o/2} v_{\text{am}}(t)^2 dt$$

$$= \begin{cases} \frac{1}{\pi} \left[\int_0^{\pi/2} \left(\frac{2}{\pi} k_t \theta \right)^2 d\theta + \int_{\pi/2}^{\pi} \left(-\frac{2}{\pi} k_t (\theta - \pi/2) \right)^2 d\theta \right] = \frac{1}{3} k_t^2 & \text{if } 0 < k_t \leq 1 \\ \frac{1}{\pi} \left[\int_0^{\pi/2k_t} \left(\frac{2}{\pi} k_t \theta \right)^2 d\theta + \int_{\pi/2k_t}^{\pi - \pi/2k_t} 1^2 d\theta + \int_{\pi - \pi/2k_t}^{\pi} \left(\frac{2}{\pi} k_t (\theta - \pi + \pi/2k_t) \right)^2 d\theta \right] = 1 - \frac{2}{3k_t} & \text{if } k_t > 1 \end{cases} \quad (16)$$

$$V_{\text{trap_1rms}} = \frac{1}{\sqrt{2}} \cdot \frac{2}{T_o} \int_0^{T_o/2} v_{\text{am}}(t) e^{-j\omega_o t} dt = \frac{1}{\sqrt{2}\pi} \int_0^{\pi/2} v_{\text{am}}(\theta) e^{-j\theta} d\theta$$

$$= \begin{cases} \frac{8k_t}{\sqrt{2}\pi^2} & \text{if } 0 < k_t \leq 1 \\ \frac{8k_t}{\sqrt{2}\pi^2} \sin\left(\frac{\pi}{2k_t}\right) & \text{if } k_t > 1 \end{cases} \quad (17)$$

Thus, the THD of v_{am} under the trapezoidal PWM method is readily obtained as follows.

$$\text{THD}_{\text{trap}} = \sqrt{\frac{V_{\text{trap_rms}}^2}{V_{\text{trap_1rms}}^2} - 1} = \begin{cases} \sqrt{\frac{\pi^4}{96} - 1} \approx 12.115\% & \text{if } 0 < k_t \leq 1 \\ \sqrt{\frac{\pi^4 (3k_t - 2)}{96k_t^3 \sin^2(\pi/2k_t)} - 1} & \text{if } k_t > 1 \end{cases} \quad (18)$$

For the modified sinusoidal PWM methods, the RMS values of the waveform (expressed in (11)) and its fundamental component are as follows.

$$V_{\text{sin_rms}}^2 = \frac{2}{T_o} \int_0^{T_o/2} v_{\text{am}}(t)^2 dt$$

$$= \begin{cases} \left(\frac{m_{\text{new}}}{\sqrt{2}} \right)^2 = \frac{m_{\text{new}}^2}{2} & \text{if } m_{\text{new}} \leq m_{\text{mpk}} \\ \frac{m_{\text{mpk}}^2}{\pi} \left[\pi + \left(\left(\frac{m_{\text{new}}}{m_{\text{mpk}}} \right)^2 - 2 \right) \sin^{-1} \left(\frac{m_{\text{mpk}}}{m_{\text{new}}} \right) - \sqrt{\left(\frac{m_{\text{new}}}{m_{\text{mpk}}} \right)^2 - 1} \right] & \text{if } m_{\text{new}} > m_{\text{mpk}} \end{cases} \quad (19)$$

This article has been accepted for publication in a future issue of this journal, but has not been fully edited. Content may change prior to final publication in an issue of the journal. To cite the paper please use the doi provided on the Digital Library page.

$$\begin{aligned}
 V_{\sin_1\text{rms}} &= \frac{1}{\sqrt{2}} \cdot \frac{2}{T_0} \int_0^{T_0/2} v_{\text{am}}(t) e^{-j\omega_0 t} dt = \frac{1}{\sqrt{2}\pi} \int_0^{\pi/2} v_{\text{am}}(\theta) e^{-j\theta} d\theta \\
 &= \begin{cases} \frac{m_{\text{new}}}{\sqrt{2}} & \text{if } m_{\text{new}} \leq m_{\text{mpk}} \\ \frac{\sqrt{2}m_{\text{mpk}}}{\pi} \left[\sqrt{1 - \left(\frac{m_{\text{mpk}}}{m_{\text{new}}}\right)^2} + \left(\frac{m_{\text{new}}}{m_{\text{mpk}}}\right) \cdot \sin^{-1}\left(\frac{m_{\text{mpk}}}{m_{\text{new}}}\right) \right] & \text{if } m_{\text{new}} > m_{\text{mpk}} \end{cases} \quad (20)
 \end{aligned}$$

where $m_{\text{mpk}} \geq 1$. Therefore, the THD of v_{am} with the modified sinusoidal PWM method is as follow.

$$\text{THD}_{\sin} = \sqrt{\frac{V_{\sin_rms}^2}{V_{\sin_1\text{rms}}^2} - 1} = \begin{cases} 0; & \text{if } m_{\text{new}} \leq m_{\text{mpk}} \\ \sqrt{\frac{\pi}{2} \cdot \frac{K_1}{K_2} - 1}; & \text{if } m_{\text{new}} > m_{\text{mpk}} \end{cases} \quad (21)$$

where K_1 and K_2 are

$$\begin{aligned}
 K_1 &= \pi + \left(\left(\frac{m_{\text{new}}}{m_{\text{mpk}}} \right)^2 - 2 \right) \sin^{-1} \left(\frac{m_{\text{mpk}}}{m_{\text{new}}} \right) - \sqrt{\left(\frac{m_{\text{new}}}{m_{\text{mpk}}} \right)^2 - 1} \\
 K_2 &= \left[\sqrt{1 - \left(\frac{m_{\text{mpk}}}{m_{\text{new}}} \right)^2} + \left(\frac{m_{\text{new}}}{m_{\text{mpk}}} \right) \cdot \sin^{-1} \left(\frac{m_{\text{mpk}}}{m_{\text{new}}} \right) \right]^2 \quad (22)
 \end{aligned}$$

Note that when $m_{\text{mpk}} = 1$, (21) shows the THD of v_{am} in the normal HC-MMC, i.e., one without any FB submodules added to the main power stage; when $m_{\text{mpk}} > 1$, it shows the THD of v_{am} in the HC-MMC with mixed-submodule approach wherein a number of FB submodules are placed in the main power stage. Further, combining the THD expressions (shown in (18) and (21)) with equations (9) and (14), the relationships between THD with the converter's modulation index, m , can be established.

Fig. 4(d) shows the THD of v_{am} with these three different voltage-regulating methods. As seen from Fig. 4(d), the trapezoidal PWM method has much higher THD due to the low-frequency harmonics embedded in its reference waveform even under idealized conditions, whereas the modified sinusoidal PWM method is devoid of harmonics under idealized conditions when $m < 1.0$, and has markedly lower THD when $m < 1.1$. For modulation indices larger than approximately 1.1, these two PWM methods have nearly identical THD. Thus, the modified sinusoidal PWM method has advantages over trapezoidal PWM in both extending the linear range of the converter operation, and generating less harmonic content. Additionally, the THD for the mixed-submodule approach is lower than both the trapezoidal and the modified sinusoidal PWM methods.

This article has been accepted for publication in a future issue of this journal, but has not been fully edited.

Content may change prior to final publication in an issue of the journal. To cite the paper please use the doi provided on the Digital Library page.

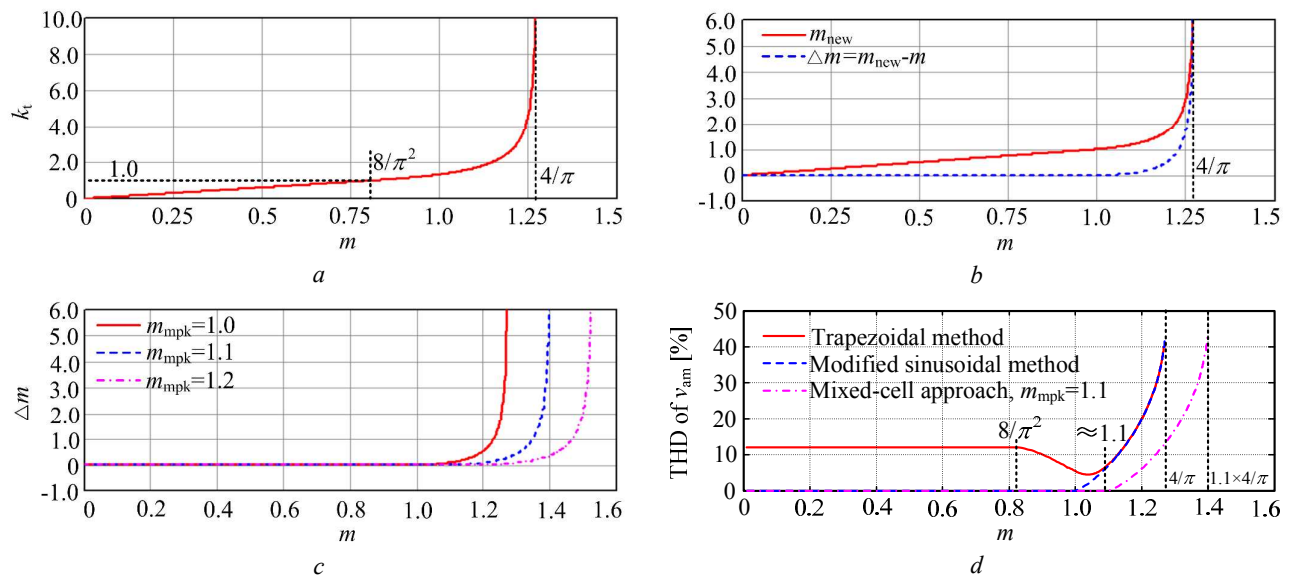


Fig. 4. Comparison of the regulation schemes

a. Trapezoidal PWM method: $k_t(m)$

b. Modified sinusoidal PWM method: $m_{new}(m)$ and $\Delta m(m)$

c. Modified sinusoidal PWM method with mixed submodules: $\Delta m(m)$ for different m_{mpk}

d. THD of voltage v_{am}

4. Experimental Verification

A downscaled laboratory setup shown in Fig. 5(a) is used to verify the ability of the discussed methods for regulating the active filter stage's FB-submodule voltages. Table 2 shows the laboratory setup specifications. The laboratory setup is controlled via a real-time digital simulator (RTDS) and feeds a passive RL load.

Table 2 Specifications of the experimental HC-MMC hardware

Parameter	Nominal value
Base frequency	60 Hz
DC voltage	120 V
No. of submodules	HB: 6/arm; FB: 3/phase
Submodule capacitance	HB: 4.7 mF; FB: 1.0 mF
Submodule capacitor voltage	HB: 20 V; FB: 20 V
For the mixed-submodule approach	FB: 1/arm; 4.7 mF and 20 V per submodule
Arm inductance	2.2 mH
Load	57 Ω and 0.23 H
Carrier frequency	main power stage: 540 Hz; active filter stage: 1620 Hz

This article has been accepted for publication in a future issue of this journal, but has not been fully edited. Content may change prior to final publication in an issue of the journal. To cite the paper please use the doi provided on the Digital Library page.

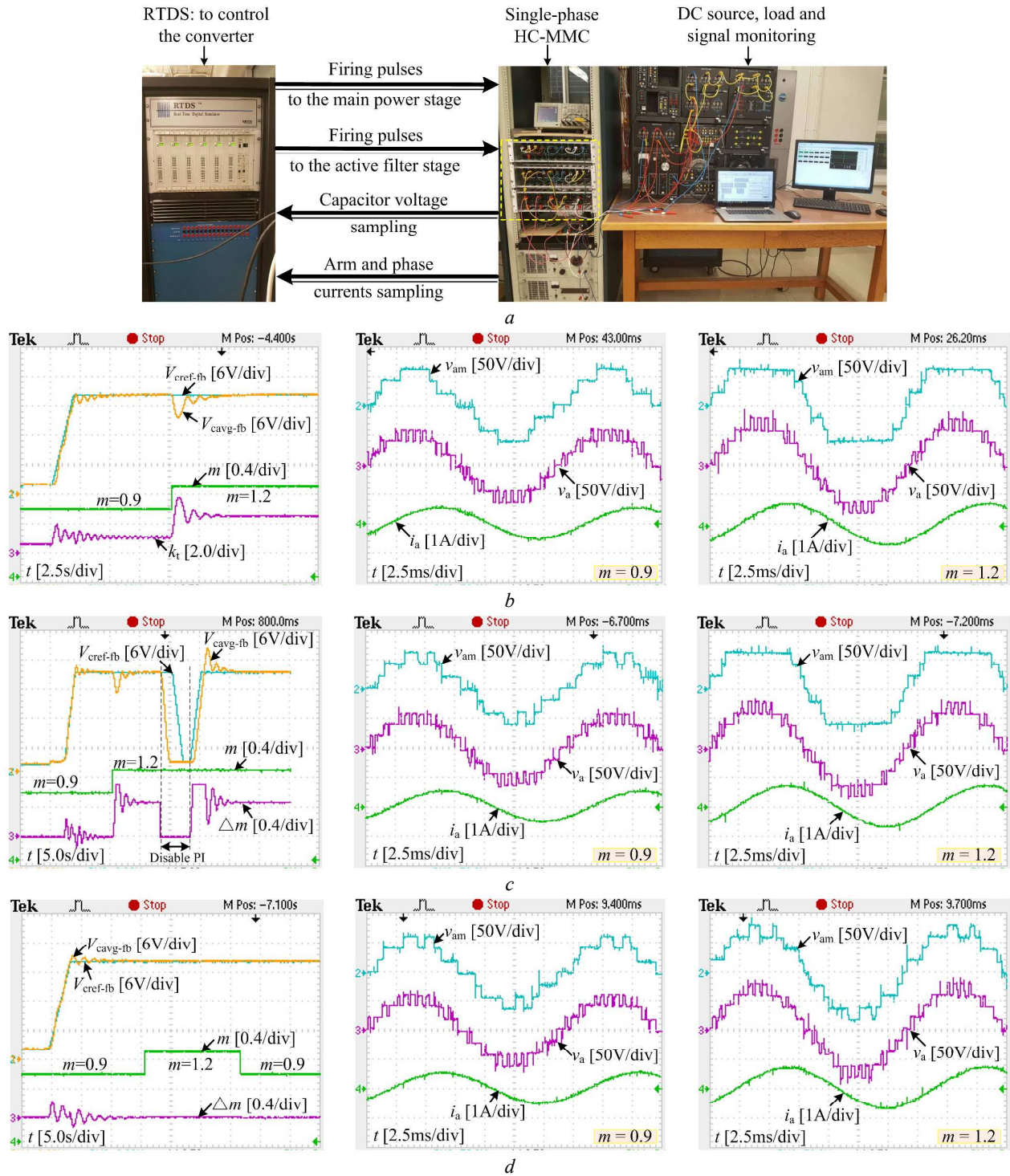


Fig. 5. Prototype of HC-MMC and experimental results with different voltage regulation methods and steady-state waveforms for $m = 0.9$ and $m = 1.2$

a. Prototype of the downscaled HC-MMC

b. Trapezoidal PWM method

c. Modified sinusoidal PWM method

d. Modified sinusoidal PWM method with mixed submodules

This article has been accepted for publication in a future issue of this journal, but has not been fully edited.

Content may change prior to final publication in an issue of the journal. To cite the paper please use the doi provided on the Digital Library page.

The experimental waveforms using the trapezoidal and modified sinusoidal PWM methods are shown in Fig. 5(b) and (c) respectively and the experimental results for the mixed-submodule method are shown in Fig. 5(d). Fig. 5 shows that the average capacitor voltage tracks the reference well for all presented methods. For the modified sinusoidal PWM method (Fig. 5(c)), the control variable Δm is nearly zero for $m = 0.9$ (within linear range). It becomes a positive value when $m = 1.2$ (within nonlinear range) in order to force the main power stage to compensate for the power delivered by the FB submodules which in turn maintains the FB-submodule voltage. To further demonstrate the regulating effect of Δm , the PI controller is deactivated momentarily as shown in Fig. 5(c) for $m = 1.2$. This causes the average FB-submodule capacitor voltage to drop, which is consistent with the analysis in Section 3.1. Upon reactivation of the PI controller, the submodule capacitor voltages are restored to their nominal value (20 V). As seen from 4(d) for the mixed-submodule approach, the variable Δm remains negligible even for the modulation index of 1.2 (compared with Fig. 5(c)), and the average capacitor voltages of the FB submodules in the active filter stage remain tightly regulated around their nominal value (20 V) while undergoing dynamic variations. This occurs because insertion of one FB submodule in series with the existing 6 HB submodules in each arm extends the linear range to approximately $(1+2 \times 1/6) \approx 1.333$. In addition, as seen from the steady-state waveforms of v_{am} and v_a shown in Figs. 5(b), (c) and (d), the individual voltage steps of both v_{am} and v_a are approximately the nominal value (20 V). Therefore, it can be concluded that the submodule capacitor voltages are well balanced.

5. Simulation-Based Case Study

A large point-to-point HVDC transmission system with a LCC rectifier and an HC-MMC inverter, shown in Fig 6(a), is used for EMT-based studies of the presented regulation schemes of Section 3. System parameters are given in Table 3 and Fig. 6(a). The dc-side parameters are adopted from CIGRE HVDC Benchmark [26] and modified for a metallic return.

Table 3 HVDC system specifications

Parameter	Nominal value
Rated power	500 MW
AC grid voltage	rectifier: 120 kV; inverter: 230 kV
Base frequency	60 Hz
DC-link voltage	500 kV
DC current	1 kA
No. of submodules	HB: 100/arm; FB: 50/phase
Submodule capacitance	HB: 5.0 mF; FB: 1.0 mF
Submodule capacitor voltage	HB: 5 kV; FB: 5 kV
For the mixed-submodule approach	FB: 5/arm; 5.0 mF and 5 kV per submodule
Arm inductance	0.05 H
Carrier frequency	main power stage: 540 Hz; active filter stage: 1620 Hz

This article has been accepted for publication in a future issue of this journal, but has not been fully edited. Content may change prior to final publication in an issue of the journal. To cite the paper please use the doi provided on the Digital Library page.

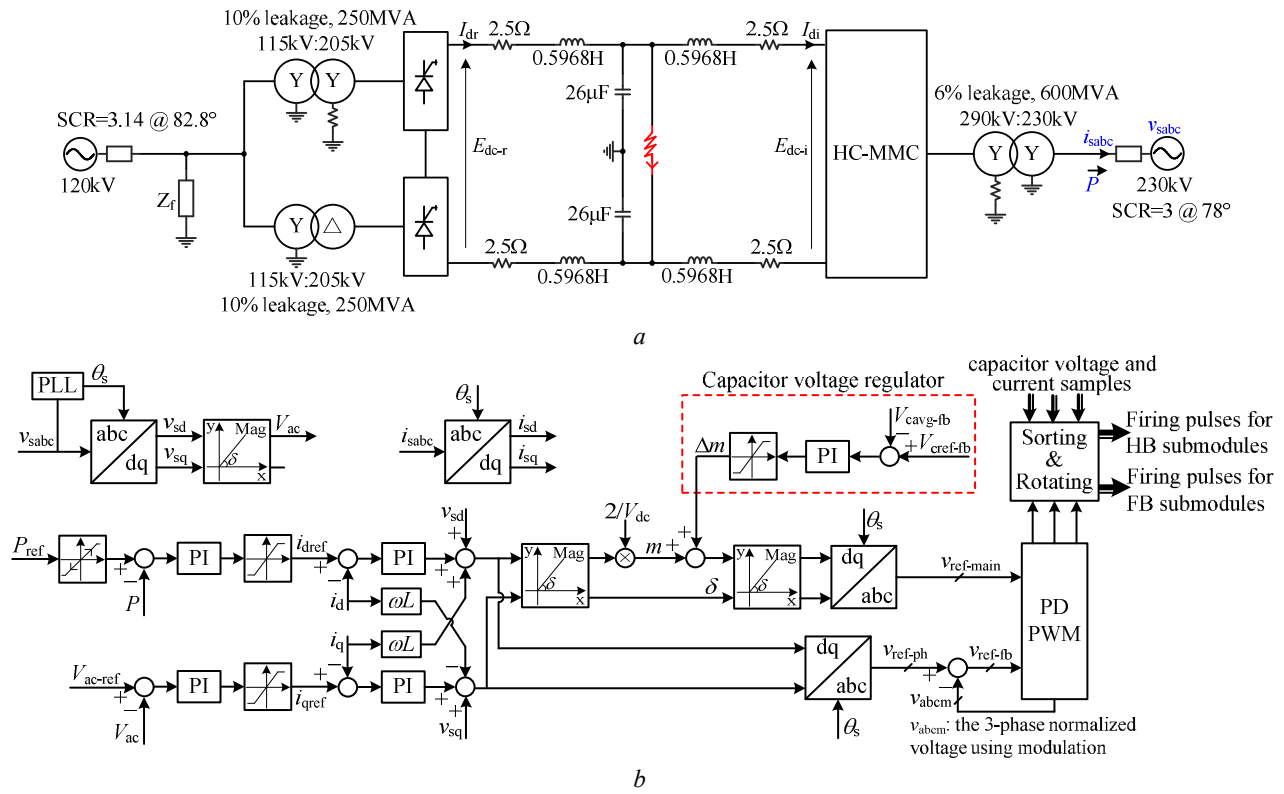


Fig. 6. LCC-HC-MMC transmission system

a. Schematic diagram

b. HC-MMC's decoupled controller + FB submodule voltage regulator

5.1. Steady-state Operation

The LCC's controller maintains the dc-link voltage, whereas the HC-MMC controls the active power and the ac voltage magnitude using decoupled control [27]. Simulation results are shown for both the trapezoidal and modified sinusoidal PWM methods. These methods are implemented for each converter phase independently, although a single-phase version is depicted in Fig. 6(b) for brevity.

Fig. 7(a) illustrates the system's response to reference variations. The power-order changes from 1.0 pu to 0.7 pu at 5 s and back to 1.0 pu at 7 s; the voltage-reference changes from 1.0 pu to 1.2 pu at 9 s and back to 1.0 pu at 12 s. It is observed that the system accurately tracks the references with reasonable transient behaviour. Additionally, the HC-MMC modulation index is ≈ 0.954 for 1.0 pu voltage magnitude reference and ≈ 1.154 for 1.2 pu.

This article has been accepted for publication in a future issue of this journal, but has not been fully edited. Content may change prior to final publication in an issue of the journal. To cite the paper please use the doi provided on the Digital Library page.

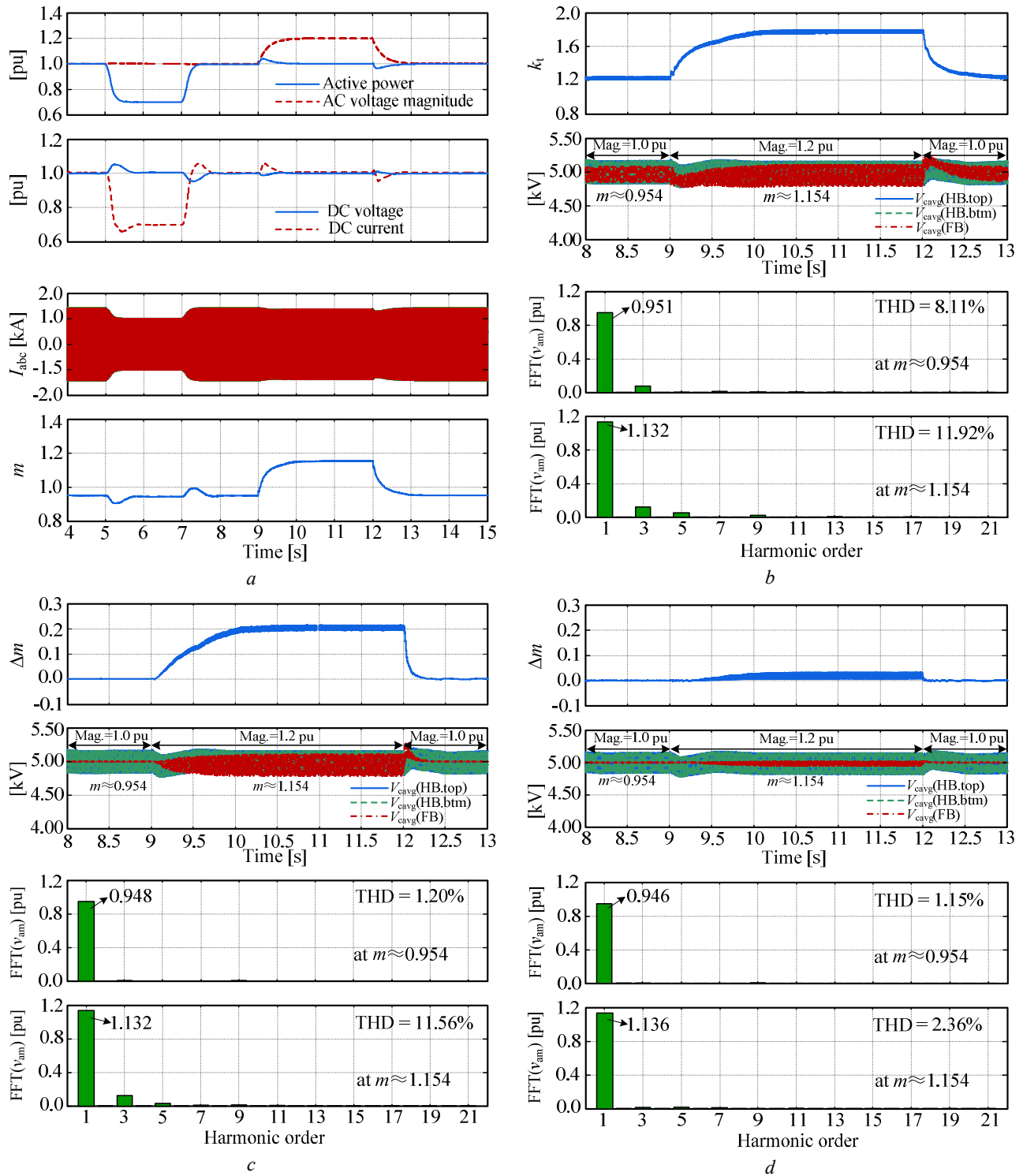


Fig. 7. Inverter-side waveforms with different voltage-regulating methods
a. Inverter-side waveforms with the modified sinusoidal PWM method
b. System response with trapezoidal PWM method
c. System response with modified sinusoidal PWM method
d. System response with mixed submodules and modified sinusoidal PWM method

This article has been accepted for publication in a future issue of this journal, but has not been fully edited.

Content may change prior to final publication in an issue of the journal. To cite the paper please use the doi provided on the Digital Library page.

Based on the same reference changes, simulation results for the trapezoidal PWM, modified sinusoidal PWM, and mixed-submodule approaches are shown in Fig. 7(b), (c) and (d), respectively. As seen from Fig. 7(c), it is observed that with the modified sinusoidal method, the required adjustment of the main power stage's modulation index (Δm) is approximately zero when the HC-MMC operates with $m \approx 0.954$ (voltage reference = 1.0 pu), and increases to 0.2 when $m \approx 1.154$ (voltage reference = 1.2 pu). In addition, the average capacitor-voltages of the active filter stage FB submodules are tightly regulated to 5 kV as desired. Since harmonics are introduced for operation with $m > 1.0$ and must be filtered by the FB submodules, the average capacitor voltage of the active filter stage FB submodules have larger ripple compared with $m < 1.0$.

In comparison, the trapezoidal PWM method always introduces low-order harmonics in the main power stage voltage, and as such the ripple of the average capacitor voltage of FB submodules is larger for modulation index of 0.954 as shown in Fig. 7(b) compared to Fig. 7(c) for the modified sinusoidal PWM method and Fig. 7(d) for the mixed-submodule method.

The HC-MMC is also simulated with combined HB and FB cells in the main power stage. Five FB submodules are added to each arm in the main power stage, corresponding to a 5% increase in the submodule count and a 10% increase in the linear range. Fig. 7(d) shows that the required Δm to produce an output voltage of 1.0 pu (for $t < 9.0$ s) is negligible with the modulation index of 0.954, and is far less than the adjustment in Fig. 7(c) for modulation index of 1.154 due to the extended linear range. The ripple of the FB-submodule average capacitor voltage (Fig. 7(d)) is smaller than the HC-MMC with only HB submodules in the main power stage due to the reduced harmonic contents of the main power stage voltage.

5.2. DC-fault Performance

A pole-to-pole fault in the middle of the dc transmission line is applied at $t = 5$ s for 0.1 s. During the fault, the LCC employs forced-retard [28] while the HC-MMC is blocked and its power-order is reduced to zero. Upon dc-fault clearing, the system resumes normal operation by ramping the power-order to the pre-fault value (Fig. 8(b)) and de-blocking the HC-MMC. As illustrated in Fig. 8(a) the rectifier-side dc current rapidly decays to zero due to LCC's forced-retard operation. The inverter-side ac currents are decreased quickly to zero due to the FB-submodule's ability to block the fault current as shown in Fig. 8(c). The dc current at the inverter side has a rapid initial decrease; it then circulates between the converter arms and the dc network and decays due to the line resistance. After fault clearance, the system restarts and the capacitor voltages are quickly restored to the required value (5 kV) as shown in Fig. 8(d).

This article has been accepted for publication in a future issue of this journal, but has not been fully edited.

Content may change prior to final publication in an issue of the journal. To cite the paper please use the doi provided on the Digital Library page.

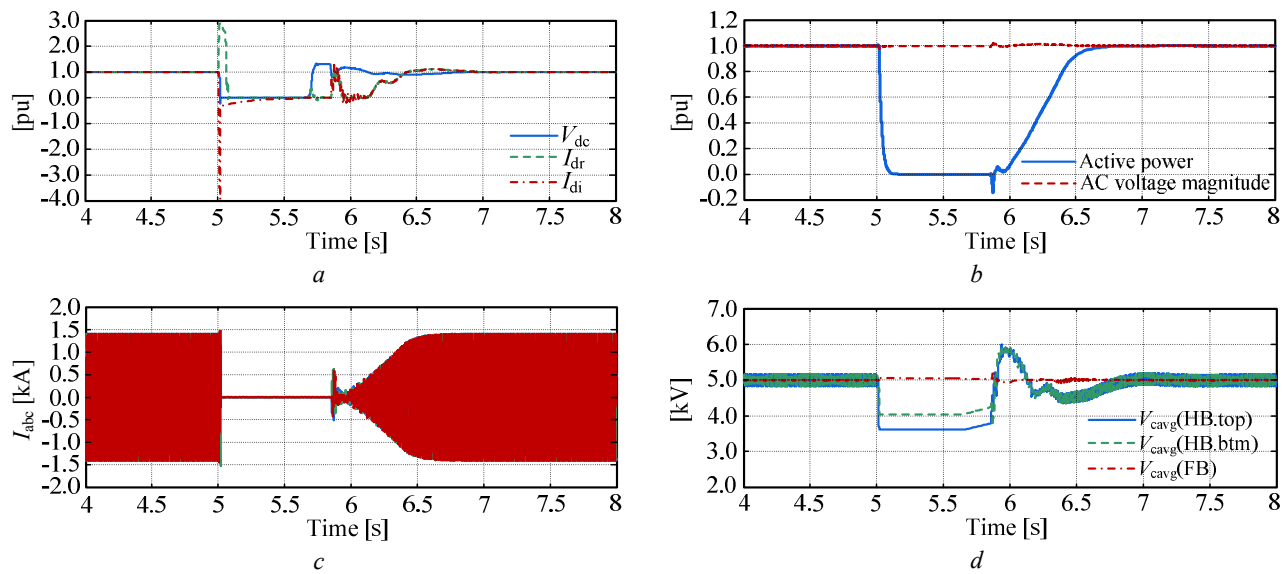


Fig. 8. Inverter response to a dc fault

a. DC voltage and current

b. Active power and ac-voltage magnitude

c. Three-phase current

d. Average capacitor voltages

6. Conclusion

This paper presented an analysis of the average power for the HC-MMC. It showed that regulation of the FB capacitor voltages requires modifications to the main power stage's control scheme. Three methods for voltage regulation were presented. The trapezoidal PWM method was shown to have a relatively small linear range ($m < 8/\pi^2 \approx 0.81$) and excessive harmonic distortion. The modified sinusoidal PWM method had an extended linear range ($m < 1.0$ or 1.15 with 3rd harmonic injection) and reduced harmonics in the linear range. A third method that involved addition of FB submodules in the main power stage was introduced, which further extended the converter's linear range (and with reduced-harmonics) in conjunction with the modified sinusoidal PWM method. The latter two methods allow the HC-MMC to be operated in an extended linear range with improved dc-link utilization and negligible harmonics. The paper also presented a detailed analysis of the harmonics generated by these methods in the form of THD figures. This is an important consideration in grid-connected operation of this converter and has wide practical benefits.

Experimental results on a scaled laboratory setup verified the efficacy of the proposed regulation methods. Extensive EMT simulations further displayed the operation and functionality of the proposed active filter stage voltage regulating methods of the HC-MMC in a large transmission system.

7. References

- [1] Debnath S., Qin J., Bahrani B., *et al.*: 'Operation, control, and applications of the modular multilevel converter: A review,' *IEEE Trans. Power Electron.*, 2015, **30**, (1), pp. 37-53.
- [2] Nami A., Liang J., Dijkhuizen F., *et al.*: 'Modular multilevel converters for HVDC applications: Review on converter cells and functionalities,' *IEEE Trans. Power Electron.*, 2015, **30**, (1), pp. 18-36.
- [3] Flourentzou N., Agelidis V. G., Demetriades G. D.: 'VSC-based HVDC power transmission systems: An overview,' *IEEE Trans. Power Electron.*, 2009, **24**, (3), pp. 592-602.
- [4] Ding G., Tang G., He Z., *et al.*: 'New technologies of voltage source converter (VSC) for HVDC transmission system based on VSC,' *Proc. IEEE Power Energy Society General Meeting*, Pennsylvania, USA, Jul. 2008, pp. 1-8.
- [5] Dorn J., Huang H., Retzmann D.: 'A new multilevel voltage-sourced converter topology for HVDC applications,' *Cigre Session*, Paris, France, Aug. 2008.
- [6] Song Q., Liu W., Li X., *et al.*: 'A steady-state analysis method for a modular multilevel converter,' *IEEE Trans. Power Electron.*, 2013, **28**, (8), pp. 3702-3713.
- [7] Hassanpoor A., Norrga S., Nami A.: 'Loss evaluation for modular multilevel converters with different switching strategies,' *ICPE-ECCE Asia*, Seoul, Korea, Jun. 2015, pp. 1558-1563.
- [8] Guan M., Xu Z., Chen H.: 'Control and modulation strategies for modular multilevel converter based HVDC System,' *Proc. Conf. IEEE Ind. Electron. Soc.*, Victoria, Australia, Nov. 2011, pp. 849-854.
- [9] Blasco-Gimenez R., Aparicio N., Ano-Villalba S., *et al.*: 'LCC-HVDC connection of offshore wind farms with reduced filter banks,' *IEEE Trans. Ind. Electron.*, 2013, **60**, (6), pp. 2372-2380.
- [10] Zhang J., Zhao C.: 'The research of SM topology with DC fault tolerance in MMC-HVDC,' *IEEE Trans. Power Delivery*, 2015, **30**, (3), pp. 1561-1568.
- [11] Wang M., Hu Y., Zhao W., *et al.*: 'Application of modular multilevel converter in medium voltage high power permanent magnet synchronous generator wind energy conversion systems,' *IET Renewable Power Generation*, 2016, **10**, (6), pp. 824-833.
- [12] Brando G., Dannier A., Pizzo A. D., *et al.*: 'Voltage fluctuation smoothing in the half-bridge cells of MMC for induction motor drives using recirculation currents SVM control,' *IEEE Int. Energy Conf.*, Dubrovnik, Croatia, 2014, pp. 94-100.
- [13] Adam G. P., Ahmed K. H., Finney S. J., *et al.*: 'New breed of network fault-tolerant voltage-source-converter HVDC Transmission System,' *IEEE Trans. Power Systems*, 2013, **28**, (1), pp. 335-346.
- [14] Adam G. P., Finney S. J., Williams B. W.: 'Hybrid converter with ac side cascaded H-bridge cells against H-bridge alternative arm modular multilevel converter: steady-state and dynamic performance,' *IET Gener. Transm. Distrib.*, 2013, **7**, (3), pp. 318-328.
- [15] Li R., Adam G. P., Holliday D., *et al.*: 'Hybrid cascaded modular multilevel converter with DC fault ride-through capability for the HVDC Transmission System,' *IEEE Trans. Power Delivery*, 2015, **30**, (4), pp. 1853-1862.
- [16] Adam G. P., Williams B. W.: 'New emerging voltage source converter for high-voltage application: hybrid multilevel converter with dc side H-bridge chain links,' *IET Gener. Transm. Distrib.*, 2014, **8**, (4), pp. 765-773.
- [17] Adam G. P., Abdelsalam I. A., Ahmed K. H., *et al.*: 'Hybrid Multilevel Converter with Cascaded H-bridge Cells for HVDC Applications: Operating Principle and Scalability,' *IEEE Trans. Power Electron.*, 2015, **30**, (1), pp. 65-77.
- [18] Xue Y., Xu Z., Tu Q.: 'Modulation and Control for a New Hybrid Cascaded Multilevel Converter with DC Blocking Capability,' *IEEE Trans. Power Delivery*, 2012, **27**, (4), pp. 2227-2237.
- [19] Adam G. P., Ahmed K. H., Williams B. W.: 'Mixed cells modular multilevel converter,' *IEEE International Symposium on Ind. Electron.*, Istanbul, Turkey, Jun. 2014, pp. 1390-1395.
- [20] Merlin M. M. C., Green T. C., Mitcheson P. D., *et al.*: 'The alternate arm converter: A new hybrid multilevel converter with DC-fault blocking capability,' *IEEE Trans. Power Delivery*, 2014, **29**, (1), pp. 310-317.
- [21] Najmi V., Burgos R., Boroyevich D.: 'Design and control of modular multilevel alternate arm converter (AAC) with zero current switching of director switches,' *IEEE Energy Conversion Congress and Exposition (ECCE)*, Montreal, Canada, Sept. 2015, pp. 6790-6797.

This article has been accepted for publication in a future issue of this journal, but has not been fully edited.

Content may change prior to final publication in an issue of the journal. To cite the paper please use the doi provided on the Digital Library page.

- [22] Saeedifard M., Iravani R.: 'Dynamic performance of a modular multilevel back-to-back HVDC system,' *IEEE Trans. Power Delivery*, 2010, **25**, (4), pp. 2903-2912.
- [23] Shi X., Filizadeh S.: 'Design Considerations of a Hybrid Cascaded Modular Multilevel Converter,' *Cigre Session*, Vancouver, Canada, Oct. 2016.
- [24] Ghat M. B., Shukla A., Mishra R.: 'A new capacitor voltage balancing control for hybrid modular multilevel converter with cascaded full bridge,' *IEEE Appl. Power Electron. Conf. and Exposition (APEC)*, Long Beach, California, Mar. 2016, pp. 2342-2348.
- [25] Li R., Fletcher J. E., Williams B. W., 'Influence of third harmonic injection on modular multilevel converter-based high voltage direct current transmission systems,' *IET Gener. Transm. Distrib.*, 2016, **10**, (11), pp. 2764-2770.
- [26] Szechtman M., Wess T., and Thio C. V., 'First benchmark model for HVDC control studies,' *Electra*, 1991, **135**, pp. 55-75.
- [27] Scahuder C., Mehta H., 'Vector analysis and control of advanced static VAR compensators,' *IEE Proceedings C – Generation, Transmission and Distribution*, 1993, **140**, (4), pp.299-306.
- [28] Barker C. D., Adamczyk A. G., Gupta R., *et al.*: 'Fault Clearing on Overhead HVDC Transmission Lines,' *Cigre Session*, Toronto, Canada, Aug. 2014.